IEEE Access
Multidisciplinary | Rapid Review | Open Access Journal

Received May 21, 2020, accepted June 5, 2020, date of publication June 15, 2020, date of current version June 24, 2020.

Digital Object Identifier 10.1109/ACCESS.2020.3002456

Position Estimation Method of IPMSM in Full Speed Range by Simplified Quadratic Optimization

FEI PENG[1], (Member, IEEE), YU YAO[1], (Graduate Student Member, IEEE), ZHIYU WANG[1], YUNKAI HUANG[1], (Member, IEEE), HUI YANG[1], (Member, IEEE), AND BINGRUO XIE[2]

[1]School of Electrical Engineering, Southeast University, Nanjing 210096, China
[2]State Key Laboratory for Traction and Control System of EMU and Locomotive, Locomotive and Car Research Institute, China Academy of Railway Sciences Corporation Ltd., Beijing 100038, China

Corresponding author: Fei Peng (pengfei@seu.edu.cn)

This work was supported by the National Natural Science Foundation of China under Grant 51777034 and Grant 51707037.

ABSTRACT In this paper, a new full-speed-range position estimation method for the interior permanent magnet synchronous machine (IPMSM) is proposed. This method is designed for high power traction motor drives. In such application, variable speed operation from zero to high speed is desired. The objective of this paper is to obtain smooth position estimation in full speed range to guarantee high reliability of the motor control system. Firstly, a quadratic cost function based on the stator voltage equations is constructed. The rotor position in the full speed range is obtained by numerically solving an optimization problem. After obtaining the rotor position, the motor speed is then obtained through a phase-locked loop observer. In such a way, only one variable in the optimization problem has to be solved. Therefore, the numeric calculation burden is greatly reduced. The convexity of the quadratic cost function considering sampling noise as well as parameter mismatch is discussed in detail. Thus, the solvability and accuracy of the estimation result is guaranteed. At last, experiments on a traction motor are conducted to verify the effectiveness of the proposed position estimation method.

INDEX TERMS IPMSM, position sensorless control, Newton method, full speed range.

I. INTRODUCTION

Due to its features of light weight, low volume, high efficiency, high torque density and wide operating speed range, Interior Permanent Magnet Synchronous Machine (IPMSM) is more and more preferred as the traction motor for automobile and railway application. To drive the IPMSM efficiently, the information of rotor position is required by the motor drive. The rotor position is often obtained by a position sensor mounted on the machine's rotor shaft. However, the hash environment of the automobile and railway application, the vibration of the motor and mechanical system increase the fault rate of the position sensor. Therefore, the position estimation method which doesn't use the position sensor is required. The estimated position can be used either to diagnose the health status of the rotor position sensor or to be fed into the motor control algorithm if fault occurs on the position sensor.

The commonly used position estimation methods for IPMSM can be divided into to two categories. One category is based on the extended back-electromotive force (Back-EMF), such as the Kalman filter method [1], [2], the model reference adaptive method [3]–[5], the observer method [6]–[9], and the artificial intelligence (AI) based method [10], [11]. Since Back-EMF is small and difficult to be observed when the rotating speed is low, these methods are only effective in the medium speed and high speed range. Another category is based on the saliency effect of the IPMSM. The inductance of the IPMSM changes according to the rotor position. High frequency voltage or current is injected into the stator to observe the rotor position [12]–[15]. Sometimes, the PWM voltage can also be taken as a kind of high frequency signal [16], [17]. This category of position estimation method is often applied at zero and low speed, when the Back-EMF is small.

The associate editor coordinating the review of this manuscript and approving it for publication was Zhilei Yao.

However, this method uses high pass filters and low pass filters to extract useful information. Therefore, the dynamic response is limited. Moreover, additional high frequency signal has to be injected into the stator, which causes additional losses and noises. Therefore, if the motor speed raises to the extent that the Back-EMF is adequately large, this category of position estimation method is then not preferred.

Normally, for the position estimation of IPMSM, the two estimation methods have to be used at the same time. A saliency effect based method is applied at zero and low speed. An extended Back-EMF based method works at medium and high speed [18]–[22]. A switching method has to be designed if the motor speed varies from low to high, or goes from high to low. If the motor speed varies often, as the traction motor in the railway application, the two estimation methods have to switch pretty often. The switching of the two independent method increases the complexity of the control algorithm. The switching may also cause oscillations on the estimated position and speed because both of the methods need initialization.

To solve the estimation method switching problem, a unified position estimation method for IPMSM in the full speed range is proposed in [23], [24]. This method obtains the rotor position and speed by solving an optimization problem using the Newton method at both low speed and high speed. No high pass or low pass filters are needed. No method switching is required. Therefore, the estimated position and speed during speed variation are smooth. However, the Hessian matrix has to be obtained by this method, which is computational complex. This method iterates both the position and speed at the same time while solving the optimization problem, thus increases the calculation burden. High performance micro-controller is required by this method. In [25], another optimization method with only one variable is formulated. Thus, obtaining the Hessian matrix is avoided and the calculation burden is reduced. However, the analysis on the convexity of the problem, the sensitivity on sampling noise and parameter mismatch are not addressed in detail.

In this paper, based on [25], an improved unified position estimation method for IPMSM with reduced numeric calculation burden is proposed. Like [23]–[25], this paper also turns the position estimation into solving an optimization problem. However, the proposed method only iterates the rotor position while solving the optimization problem. The motor speed can be estimated through a phase-locked loop (PLL) observer. In this way, the calculation burden of the micro-controller is reduced. Detailed analysis on convergence of the problem, sensitivity of sampling noise and parameter mismatch are provide to prove the feasibility of the proposed method. The effectiveness of the proposed position estimation method is then experimentally verified on a tested traction motor.

This paper is organized as follows: In Section II, the mathematical model of IPMSM used in this paper is described. Then, the proposed unified position estimation method, as well as the convexity examination under different cases are presented in Section III. The sensitivity of sampling noise and parameter mismatch are also discussed in this section. Finally, the efficient method of solving the optimization problem is given. In Section IV, the effectiveness of the proposed position and speed estimation method is experimentally tested under different speed and load. At last, conclusions are drawn in Section V.

II. MATHEMATICAL MODELING OF IPMSM

In order to demonstrate the proposed position estimation method, the model of IPMSM used in this paper have to be presented first.

The voltage equation of the IPMSM in the $\alpha\beta$ stationary coordinate is given as

$$\begin{bmatrix} u_\alpha \\ u_\beta \end{bmatrix} = R_S \begin{bmatrix} i_\alpha \\ i_\beta \end{bmatrix} + L_a(\theta_e) \begin{bmatrix} pi_\alpha \\ pi_\beta \end{bmatrix} + \omega_e L_b(\theta_e) \begin{bmatrix} i_\alpha \\ i_\beta \end{bmatrix} + \omega_e \psi_f \begin{bmatrix} -\sin(\theta_e) \\ \cos(\theta_e) \end{bmatrix} \quad (1)$$

and

$$\begin{cases} L_a(\theta_e) = \begin{bmatrix} L_1 + L_2\cos(2\theta_e) & L_2\sin(2\theta_e) \\ L_2\sin(2\theta_e) & L_1 - L_2\cos(2\theta_e) \end{bmatrix} \\ L_b(\theta_e) = 2L_2 \begin{bmatrix} -\sin(2\theta_e) & \cos(2\theta_e) \\ \cos(2\theta_e) & \sin(2\theta_e) \end{bmatrix} \end{cases} \quad (2)$$

where u_α, u_β, i_α and i_β are the voltages, currents in the $\alpha\beta$ coordinate respectively. R_S is the stator resistance. $L_1 = (L_d + L_q)/2$ and $L_2 = (L_d - L_q)/2$, where L_d and L_q are the stator inductances in the dq-axis, respectively. p is the differential operator and ω_e is the electrical angular velocity of the motor. θ_e and ψ_f are the electrical position of the rotor and permanent magnet flux linkage, respectively.

In order to implement digital control and estimation, (1) is then transformed into discrete domain by using the forward Euler method. The voltage equation of the IPMSM in discrete domain in the $\alpha\beta$ stationary coordinate is given as:

$$\begin{aligned} u_{\alpha\beta}(k) &= R_S i_{\alpha\beta}(k) + L_a(\theta_e(k)) \frac{\Delta i_{\alpha\beta}(k)}{T} \\ &\quad + \omega_e(k) L_b(\theta_e(k)) i_{\alpha\beta}(k) + \omega_e(k) \psi_f \begin{bmatrix} -\sin(\theta_e(k)) \\ \cos(\theta_e(k)) \end{bmatrix} \\ \frac{\Delta i_{\alpha\beta}(k)}{T} &= \omega_e(k) \begin{bmatrix} 0 & -1 \\ 1 & 0 \end{bmatrix} i_{\alpha\beta}(k) + \frac{i_{\alpha\beta}(k)}{T} \\ &\quad - \begin{bmatrix} \cos(\omega_e T) & -\sin(\omega_e T) \\ \sin(\omega_e T) & \cos(\omega_e T) \end{bmatrix} \frac{i_{\alpha\beta}(k-1)}{T} \end{aligned} \quad (3)$$

where $u_{\alpha\beta} = \left[u_\alpha(k)\, u_\beta(k)\right]^T$ and $i_{\alpha\beta} = \left[i_\alpha(k)\, i_\beta(k)\right]^T$ represent the voltage and current in the $\alpha\beta$ stationary coordinate, respectively. k donates the time step and T is the sampling period.

III. THE PROPOSED UNIFIED POSITION ESTIMATION IN FULL SPEED RANGE

Based on the mathematical model presented above, this paper presented a unified position estimation method in full speed

range. Firstly, since (3) is effective at both low speed and high speed, an optimization problem related to the rotor position is constructed based on (3). Then the convexity of the cost function is examined under different cases. Later, some details of the optimization problem, such as sampling noise sensitivity, injected high frequency signal at zero and low speed, as well as parameter sensitivity are presented. At last the Newton method is implemented to solve the optimization problem to obtain the rotor position.

A. CONSTRUCTION OF THE OPTIMIZATION PROBLEM

A cost function G is constructed based on (3):

$$\begin{aligned} & f_e\left(\hat{\theta}_e(k), \hat{\omega}_e(k)\right) \\ & = u_{\alpha\beta}(k) - R_S i_{\alpha\beta}(k) \\ & \quad - L_a\left(\hat{\theta}_e(k)\right)\frac{\Delta i_{\alpha\beta}(k)}{T} - \hat{\omega}_e(k) L_b\left(\hat{\theta}_e(k)\right) i_{\alpha\beta}(k) \\ & \quad - \hat{\omega}_e(k)\psi_f \begin{bmatrix} \sin\left(\hat{\theta}_e(k)\right) \\ -\cos\left(\hat{\theta}_e(k)\right) \end{bmatrix} \\ & \quad \times G\left(\hat{\theta}_e(k), \hat{\omega}_e(k)\right) = \left\| f_e\left(\hat{\theta}_e(k), \hat{\omega}_e(k)\right)\right\|^2 \end{aligned} \tag{4}$$

where $\hat{\theta}_e$ and $\hat{\omega}_e$ are the estimated value of the position and electrical angular velocity. $\|\cdot\|$ is the norm operation. Equation (4) shows that there are only two unknown parameters in G. If the IPMSM parameters are accurately known and the sampling of voltage and current are accurate, then, the value of the cost function will be zero when the estimated position and velocity equal to their actual values.

Based on above points, the position and velocity estimation can be obtained by solving $G = 0$. However, the process of directly solving $G = 0$ is complicated and is difficult to implement. In order to simplify the solution, the problem can be transformed to an optimization problem and then is solved by nonlinear optimization algorithm. The estimated position and velocity values that make G the minimum are the finally estimated position and velocity of the IPMSM:

$$\min_{\hat{\theta}_e(k),\hat{\omega}_e(k)} G\left(\hat{\theta}_e(k), \hat{\omega}_e(k)\right) \tag{5}$$

Moreover, if the estimated position $\hat{\theta}_e(k)$ is obtained, the estimated angular speed $\hat{\omega}_e(k)$ could be obtained by feeding $\hat{\theta}_e(k)$ into a PLL observer. If the dynamic of the observer is fast enough, there will be $\omega_e(k) \approx \hat{\omega}_e(k)$. In this case, the optimization could be simplified as:

$$\min_{\hat{\theta}_e(k)} G\left(\hat{\theta}_e(k), \omega_e(k)\right) \tag{6}$$

In (6), only one variable has to be optimized, which greatly reduces the computation burden of the digital controller.

B. PLL OBSERVER FOR SPEED ESTIMATION

Since the rotor position and angular speed are not independent, the ω_e needed by (6) could be estimated from a simple PLL observer. In this way, the computation burden of solving the optimization problem is reduced.

FIGURE 1 shows the structure of the proposed rotor position and angular speed estimation method. The position estimated by the PLL observer $\hat{\theta}_{PLL}(k)$ is compared with the position estimated by solving the optimization problem $\hat{\theta}_e(k)$. A PI regulator then takes the difference to calculate the estimated angular speed $\hat{\omega}_e(k)$. The rotor position of the next sampling step $\hat{\theta}_{PLL}(k+1)$ is predicted with a simple integrator. $\hat{\theta}_{PLL}(k+1)$ can also be used as the initial point for solving the optimization problem at next sampling period. Since the sampling frequency is usually high, angular speed changes relative slow. Therefore, $\hat{\theta}_{PLL}(k+1)$ is very close to the optimal solution $\hat{\theta}_e(k+1)$ of the next step. In such a way, the iteration step could be reduced. It has to be noted that, since the estimated angular speed $\hat{\omega}_e(k)$ is only known after $\hat{\theta}_e(k)$ is obtained, $\hat{\omega}_e(k-1)$ is used instead of $\hat{\omega}_e(k)$ for solving the optimization problem. If the angular speed changes slow with regard to the sampling frequency, the replacement is feasible.

The performance of the PLL observer is determined by its transfer function and it is easy to be designed using conventional linear control theory.

C. CONVEXITY EXAMINATION OF THE COST FUNCTION

The optimization problem can be solved only if the the cost function is at least locally convex. Therefore, before applying the proposed method, the convex examination has to be performed.

1) ZERO AND LOW SPEED

If the angular speed is as low as zero, the term associated with ω_e in (4) could be neglected. The cost function could be rewritten as

$$\begin{aligned} f_e\left(\hat{\theta}_e(k), 0\right) &= u_{\alpha\beta}(k) - R_S i_{\alpha\beta}(k) \\ &\quad - L_a\left(\hat{\theta}_e(k)\right)\frac{\Delta i_{\alpha\beta}(k)}{T} \\ G\left(\hat{\theta}_e(k), 0\right) &= \left\| f_e\left(\hat{\theta}_e(k), 0\right)\right\|^2 \end{aligned} \tag{7}$$

substituting (3) into (7), there is

$$G\left(\hat{\theta}_e(k)\right) = \left\| \left(L_a(\theta_e(k)) - L_a\left(\hat{\theta}_e(k)\right)\right)\frac{\Delta i_{\alpha\beta}(k)}{T}\right\|^2 \tag{8}$$

It is clear that if the term $\Delta i_{\alpha\beta}(k)$ is zero, $G\left(\hat{\theta}_e(k)\right)$ is always zero. Thus, the optimization problem can't be solved. If the term $\Delta i_{\alpha\beta}(k)$ is not zero, $G\left(\hat{\theta}_e(k)\right)$ will be zero if $\hat{\theta}_e = \theta_e$, thus the optimization is solved. In order to keep the term $\Delta i_{\alpha\beta}(k)$ not being zero, high frequency current has to be injected into the stator when the motor speed is low or zero. After the current injection, (8) becomes

$$G\left(\hat{\theta}_e(k)\right) = 4L_2{}^2 \sin^2\left(\tilde{\theta}_e(k)\right) \Delta i_{\alpha\beta}{}^T \Delta i_{\alpha\beta} \Big/ T^2 \tag{9}$$

where

$$\tilde{\theta}_e(k) = \theta_e(k) - \hat{\theta}_e(k) \tag{10}$$

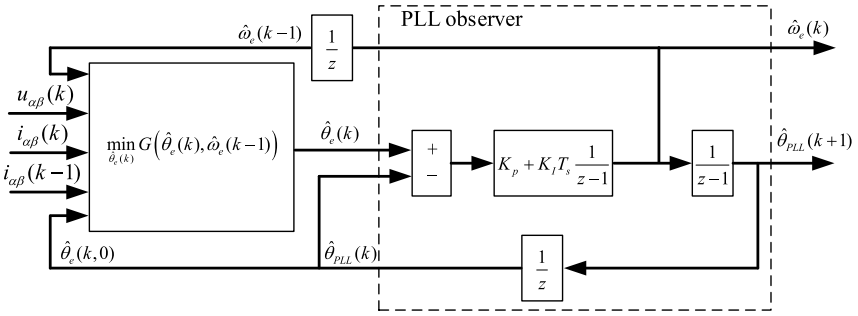

FIGURE 1. Structure of the proposed rotor position and angular speed estimation method.

It is clear that (9) is a periodic function with period π. With any estimated rotor position $\hat{\theta}_e$, $G\left(\hat{\theta}_e(k)\right)$ is locally convex in the range $[\theta_e - \pi/2 + n\pi, \theta_e + \pi/2 + n\pi]$, $n = \pm1, \pm2, \pm3, \ldots$, thus the optimization could be solved. And the result will be $\hat{\theta}_e = \theta_e$, or $\hat{\theta}_e = \theta_e + n\pi$. Therefore the correct solution of the $\hat{\theta}_e(k)$ can only be obtained if the initial value of $\hat{\theta}_e(k)$ in the iteration is $\pm\pi/2$ close to $\theta_e(k)$. Otherwise, $\hat{\theta}_e(k)$ will converge to another solution which is π away from the $\theta_e(k)$. In this paper, the conventional polarity determination is performed to determine the initial value of the $\hat{\theta}_e(k)$ in the iteration.

2) MEDIUM AND HIGH SPEED

If the motor speed goes higher, ω_e is not zero. The value of $G\left(\hat{\theta}_e(k), \omega_e(k)\right)$ will change according to $\hat{\theta}_e(k)$ even if no additional high frequency current is injected into the stator winding. Then, substituting (3) into (4), there will be

$$\begin{aligned} & f_e\left(\hat{\theta}_e(k), \omega_e(k)\right) \\ & = L_2 \begin{bmatrix} \tilde{\cos}\left(2\theta_e(k)\right) & \tilde{\sin}\left(2\theta_e(k)\right) \\ \tilde{\sin}\left(2\theta_e(k)\right) & -\tilde{\cos}\left(2\theta_e(k)\right) \end{bmatrix} \frac{\Delta i_{\alpha\beta}(k)}{T} \\ & \quad + 2L_2\omega_e(k) \begin{bmatrix} -\tilde{\sin}\left(2\theta_e(k)\right) & \tilde{\cos}\left(2\theta_e(k)\right) \\ \tilde{\cos}\left(2\theta_e(k)\right) & \tilde{\sin}\left(2\theta_e(k)\right) \end{bmatrix} i_{\alpha\beta}(k) \\ & \quad + \omega_e(k)\psi_f \begin{bmatrix} -\sin\left(\theta_e(k)\right) + \sin\left(\hat{\theta}_e(k)\right) \\ \cos\left(\theta_e(k)\right) - \cos\left(\hat{\theta}_e(k)\right) \end{bmatrix} \\ & \quad \times G\left(\hat{\theta}_e(k), \omega_e(k)\right) = \left\| f_e\left(\hat{\theta}_e(k), \omega_e(k)\right) \right\|^2 \end{aligned} \tag{11}$$

where

$$\begin{aligned} \tilde{\sin}\left(2\theta_e(k)\right) &= \sin\left(2\theta_e(k)\right) - \sin\left(2\hat{\theta}_e(k)\right) \\ \tilde{\cos}\left(2\theta_e(k)\right) &= \cos\left(2\theta_e(k)\right) - \cos\left(2\hat{\theta}_e(k)\right) \end{aligned} \tag{12}$$

For most motors, L_2 is usually small, and the back-EMF is the most significant term in $f_e\left(\hat{\theta}_e(k), \omega_e(k)\right)$ at high speed. Therefore, if the term associated with L_2 is neglected, $G\left(\hat{\theta}_e(k), \omega_e(k)\right)$ becomes:

$$\begin{aligned} & G\left(\hat{\theta}_e(k), \omega_e(k)\right) \\ & \approx \left\| \omega_e(k)\psi_f \begin{bmatrix} -\left(\sin\left(\theta(k)\right) - \sin\left(\hat{\theta}_e(k)\right)\right) \\ \cos\left(\theta(k)\right) - \cos\left(\hat{\theta}_e(k)\right) \end{bmatrix} \right\|^2 \\ & = \left(2\omega_e(k)\psi_f\right)^2 \sin^2\left(\frac{\tilde{\theta}_e(k)}{2}\right) \end{aligned} \tag{13}$$

It is shown from (13) that $G\left(\hat{\theta}_e(k), \omega_e(k)\right)$ is a periodic function with period 2π and is convex between $[0, 2\pi]$. Therefore, the rotor position could be obtained at any θ_e by solving the optimization function.

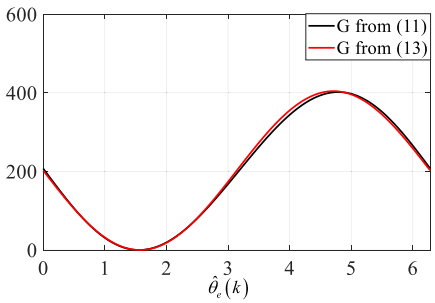

FIGURE 2. The waveform of $G\left(\hat{\theta}_e(k), \omega_e(k)\right)$ at position $\pi/2$ rad and rated speed.

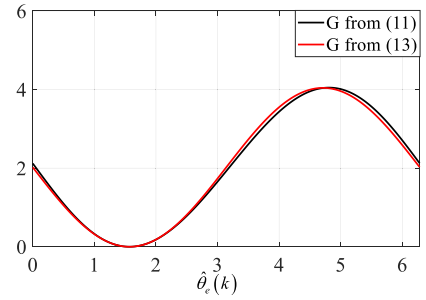

FIGURE 3. The waveform of $G\left(\hat{\theta}_e(k), \omega_e(k)\right)$ at position $\pi/2$ rad and 10% of the rated speed.

FIGURE 2, FIGURE 3 show the value of $G\left(\hat{\theta}_e(k), \omega_e(k)\right)$ calculated by (11) and (13) at the rated speed and 10% of the

rated speed with rated current. It is shown that the shapes of (4) at different speed are all convex in the range $[0, 2\pi)$. And there is little difference between the results from (11) and (13). Thus, the rotor position could be estimated by solving the optimization problem. In addition, the maximum value of G increases as the speed increases. This feature indicates that this method has stronger robustness at higher speed.

3) LOW SPEED

At low speed, the situation becomes complex. Both Back-EMF and current injection exits. None of the terms in (11) could be neglected, which makes the analyzing complex. To analyze the cost function, (11) is Taylor expanded around θ_e:

$$G\left(\hat{\theta}_e(k), \hat{\omega}_e(k)\right) = A\left(\theta_e(k)\right)\tilde{\theta}_e(k)^2 \tag{14}$$

where $A\left(\theta_e(k)\right)$ is the slope of $G\left(\hat{\theta}_e(k), \omega_e(k)\right)$ at $\theta_e(k)$:

$$\begin{aligned} &A\left(\theta_e(k)\right) \\ &= \left\| \begin{array}{l} 4L_2\omega_e(k)\begin{bmatrix} \cos\left(2\theta_e(k)\right) & \sin\left(2\theta_e(k)\right) \\ \sin\left(2\theta_e(k)\right) & -\cos\left(2\theta_e(k)\right) \end{bmatrix} i_{\alpha\beta}(k) \\ +2L_2\begin{bmatrix} \sin\left(2\theta_e(k)\right) & -\cos\left(2\theta_e(k)\right) \\ -\cos\left(2\theta_e(k)\right) & -\sin\left(2\theta_e(k)\right) \end{bmatrix} \dfrac{\Delta i_{\alpha\beta}(k)}{T} \\ +\psi_f\omega_e(k)\begin{bmatrix} \cos\left(\theta_e(k)\right) \\ \sin\left(\theta_e(k)\right) \end{bmatrix} \end{array} \right\|^2 \end{aligned} \tag{15}$$

FIGURE 4 shows the waveform of $G\left(\hat{\theta}_e(k), \omega_e(k)\right)$ calculated from (11) and (14) at position $\pi/2$ rad with 10% and 2% of the rated speed. Where F_N is the rated working frequency. It is shown from both (14) and FIGURE 4 that $G\left(\hat{\theta}_e(k), \omega_e(k)\right)$ is locally convex near $\theta_e(k)$ with any speed and current as long as $A\left(\theta_e(k)\right)$ is not zero. Therefore the rotor position could be obtained by solving the optimization problem as long as the initial value of $\hat{\theta}_e(k)$ is close to $\theta_e(k)$. This condition could be easily satisfied as long as the correct rotor position is obtained at zero speed while starting up.

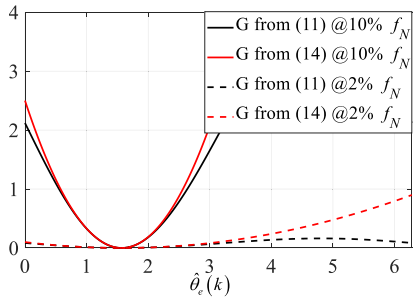

FIGURE 4. The waveform of $G\left(\hat{\theta}_e(k), \omega_e(k)\right)$ at position $\pi/2$ rad and 10% and 2% of the rated speed.

D. SAMPLING NOISE SENSITIVITY

The analyze above are all based on ideal situation, which means all the sampled variable and motor parameters are assumed accurate. However, in real implementation, there may be noise in the sampled variables. The process of current sampling and PWM output could bring noise to the $i_{\alpha\beta}$ and $u_{\alpha\beta}$, respectively. In voltage equation (1), the current noise will eventually turn to voltage noise. Therefore, the sampling noise on current and voltage could be expressed by a lumped noise voltage $\Delta u_{\alpha\beta} = \left[\Delta u_\alpha \Delta u_\beta\right]^T$. The error caused by discretization from (1) to (3) could be also included in $\Delta u_{\alpha\beta}$.

1) ZERO SPEED

Considering $\Delta u_{\alpha\beta}$, (8) becomes:

$$\begin{aligned} &G\left(\hat{\theta}_e(k)\right) \\ &= \left\| \left(L_a\left(\theta_e(k)\right) - L_a\left(\hat{\theta}_e(k)\right)\right)\frac{\Delta i_{\alpha\beta}(k)}{T} + \Delta u_{\alpha\beta}(k) \right\|^2 \end{aligned} \tag{16}$$

Considering the high frequency current injection, (16) will eventually become:

$$\begin{aligned} &G\left(\hat{\theta}_e(k)\right) \\ &= 4L_2{}^2\sin^2\left(\tilde{\theta}_e(k)\right)\Delta i_{\alpha\beta}{}^T\Delta i_{\alpha\beta}\Big/T^2 + \left\|\Delta u_{\alpha\beta}\right\|^2 \\ &\quad + 2A_nL_2\cdot\left(\cos\left(2\theta_e(k) - \theta_n\right) - \cos\left(2\hat{\theta}_e(k) - \theta_n\right)\right) \end{aligned} \tag{17}$$

where

$$A_n = \sqrt{\left\|\Delta u_{\alpha\beta}\right\|^2\Delta i_{\alpha\beta}{}^T\Delta i_{\alpha\beta}\Big/T^2} \tag{18}$$

and θ_n is the angle caused by the noise. θ_n will be random if the noise is random.

It is shown from (17) that $G\left(\hat{\theta}_e(k)\right)$ can no longer reach zero, and the optimal solution for $\hat{\theta}_e(k)$ is no longer the real rotor position $\theta_e(k)$. The difference between the optimized $\hat{\theta}_e(k)$ and $\theta_e(k)$ is

$$\frac{1}{2}\arctan\left(\frac{\sin\left(2\theta_e(k) - \theta_n\right)}{\dfrac{L_2\sqrt{\Delta i_{\alpha\beta}{}^T\Delta i_{\alpha\beta}/T^2}}{\left\|\Delta u_{\alpha\beta}\right\|} - \cos\left(2\theta_e(k) - \theta_n\right)}\right) \tag{19}$$

It is indicated from (19) that, in order to reduce the position error $\Delta\theta_e(k)$, the amplitude of noise has to be reduced. Otherwise, the amplitude of the injected current has to be selected as large as possible. According to (9), the amplitude of the injected current actually determines the slope of $G\left(\hat{\theta}_e(k)\right)$. This means the larger the slope is, $\hat{\theta}_e(k)$ is the less sensitive to noise.

2) HIGH SPEED

Adding $\Delta u_{\alpha\beta}$ into (13), the estimated position error caused by sampling could be expressed as

$$\Delta\theta_e(k) = \arctan\frac{\cos\left(\theta_e(k) - \theta_n\right)}{\dfrac{2\psi_f\omega_e(k)}{\left\|\Delta u_{\alpha\beta}\right\|} - \sin\left(\theta_e(k) - \theta_n\right)} \tag{20}$$

It is shown from (20) that, in order to reduce the position error $\Delta\theta_e(k)$, the amplitude of noise should be reduced.

Otherwise, the term $\psi_f \omega_e(k)$, which is the back-EMF, should be as large as possible. This means the estimated position is less sensitive to sampling noise at higher speed.

It has to be noted that even though the sampling noise could bring error to the estimated position, however, by properly designing the bandwidth of the PLL observer, the effect of sampling noise will be significantly attenuated.

E. THE INJECTED HIGH FREQUENCY SIGNAL AT ZERO AND LOW SPEED

At low speed, even though $G\left(\hat{\theta}_e(k), \omega_e(k)\right)$ is still convex, however, both its value and slope get smaller as the speed decreases. The noise on current and voltage signals is easy to bring errors on the estimated position. In order to keep good estimation accuracy against noise, the amplitude of $A(\theta_e(k))$ in (14) has to be kept as large as possible. Therefore the high frequency current or voltage signal has to be injected and $A(\theta_e(k))$ has to be carefully analyzed. At low speed, the term $\omega_e(k)$ is small, therefore, the term associated with $L_2\omega_e(k)$ is assumed to be neglected, then $A(\theta_e(k))$ becomes

$$A(\theta_e(k)) \approx 4{L_2}^2 \Delta {i_{\alpha\beta}}^T \Delta i_{\alpha\beta} \Big/ T^2 + {\psi_f}^2\omega^2 + 4L_2\psi_f\omega\Delta {i_{\alpha\beta}}^T \Big/ T \begin{bmatrix} \sin(\theta_e(k)) \\ -\cos(\theta_e(k)) \end{bmatrix} \quad (21)$$

In order to keep $A(\theta_e(k))$ constant at any position, the last term of $A(\theta_e(k))$ in (21) has to be kept at zero. To achieve this purpose, in this paper, there is

$$\left|\Delta i_{\alpha\beta}\right| = \Delta I_H \begin{bmatrix} \cos\left(\hat{\theta}_e(k)\right) \\ \sin\left(\hat{\theta}_e(k)\right) \end{bmatrix} \quad (22)$$

After $\hat{\theta}_e(k)$ approximates $\theta_e(k)$, $A(\theta_e(k))$ will become $4{L_2}^2\Delta {I_H}^2 \big/ T^2 + {\psi_f}^2\omega^2$, which is constant. The amplitude of $A(\theta_e(k))$ is determined by ΔI_H as well as the back-EMF.

Transforming (22) into the estimated dq coordinate, there will be:

$$\left|\Delta i_{dq}\right| = \Delta I_H \begin{bmatrix} 1 \\ 0 \end{bmatrix} \quad (23)$$

This indicates the current variation every sampling period should be ΔI_H. An additional square voltage wave with amplitude being $L_d\Delta I_H/T$ should be added to the d-axis to achieve this goal. The frequency of the injected voltage wave does not influence $\left|\Delta i_{dq}\right|$. Nevertheless, higher voltage frequency will lead to lower amplitude of current ripple. The value of ΔI_H determines the amplitude of A, and according to (19), It should be as large as possible to reduce the position estimation error caused by noise. However, larger current variation will cause more power loss and acoustic noise. In this paper, if the amplitude of current sampling noise is I_{noise}, ΔI_H is recommended to be

$$\Delta I_H \geq 4\frac{max(L_d, L_q)}{|L_2|} \times I_{noise} \quad (24)$$

Thus, according to (19), the position estimation error caused by noise is bounded within $\pi/8$ rad.

On the other hand, producing the current variation of ΔI_H need sufficient voltage supply. Thus, there should be

$$\Delta I_H \leqslant \frac{T}{L_d}\sqrt{\left(80\%\frac{V_{DC}}{2}\right)^2 - (\omega_B\psi)^2} \quad (25)$$

where ω_B is the boundary between high speed and low speed. V_{DC} is the DC bus voltage.

As the motor speed gets higher, the back-EMF term in (21) rises. The high frequency signal injection is then no longer needed. According to (20), ω_B has also to be selected according to the sampling noise level of the system to guarantee bounded position estimation error. For example, the voltage noise level $\left\|\Delta u_{\alpha\beta}\right\|$, which includes the DC bus sampling error, the PWM output error, and the current sampling error, could be limited below 4% of V_{DC} in a normal motor drive system. Thus, ω_B is recommended to be $4\%V_{DC}/\psi_f$, so that the position estimation error caused be noise is bounded within $\pi/8$ rad. This means if the rated back-EMF of the motor is designed around $V_{DC}/2$, the high frequency signal injection could stop at about 8% of the motor's rated speed. Note that if the noise level of the motor is reduced, the ω_B could be selected even smaller. It is recommended that a transition speed range should be set around ω_B so that the high frequency current is added or canceled gradually instead of in sudden.

F. PARAMETER SENSITIVITY

In digital implementation, the parameters of the motor adopted in the controller may not exactly match the parameters of the real motor. The mismatch of the inductance may cause position estimation error at zero and low speed, since the back-EMF is low. The estimated angular speed $\hat{\omega}_e$ may not match the real angular speed ω_e, especially during the dynamic response. This may also bring position estimation error.

1) ZERO SPEED

At zero speed, the term of back-EMF is low and is neglected. Therefore, only the mismatch on inductance and resistance are studied.

Mismatch of L_2:

Firstly, it is assumed at L_1 is accurate, there is only mismatch in L_2. Then (8) becomes

$$G\left(\hat{\theta}_e(k)\right) \approx \frac{\Delta {I_H}^2}{T^2}\begin{pmatrix} 4{L_2}^2\left(\sin\left(\theta_e(k) - \hat{\theta}_e(k)\right)\right)^2 + \Delta {L_2}^2 \\ +4L_2\Delta L_2\left(\sin\left(\theta_e(k) - \hat{\theta}_e(k)\right)\right)^2 \end{pmatrix} \quad (26)$$

where ΔL_2 is the difference between the real L_2 and that used in the controller. It is shown from (26) that even though $G\left(\hat{\theta}_e(k)\right)$ will no longer reach zero with the mismatched inductance, however, the optimal solution for $\hat{\theta}_e(k)$ is still $\theta_e(k)$. Thus, mismatched L_2 will not bring in position estimation error. However, it is shown that too large mismatch

may reduce the slope of $G\left(\hat{\theta}_e(k)\right)$, therefore ΔL_2 should be carefully measured.

Mismatch of L_1:

If there is mismatch in L_1 while L_2 is accurate in the digital controller. Then (8) becomes

$$\begin{aligned} &G\left(\hat{\theta}_e(k)\right) \\ &\approx \Delta {L_1}^2 \Delta {I_H}^2 \Big/ T^2 \\ &\quad +4L_2\left(L_2-\Delta L_1\right)\Delta {I_H}^2 \Big/ T^2\left(\sin\left(2\theta_e(k)-2\hat{\theta}_e(k)\right)\right)^2 \end{aligned} \tag{27}$$

where ΔL_1 is the difference between the real L_1 and that used in the controller. It is shown that if there is mismatch in L_1, the optimal solution for $\hat{\theta}_e(k)$ is still $\theta_e(k)$. However, it has be to noted that too large ΔL_1 may reduce the slope of $G\left(\hat{\theta}_e(k)\right)$ or even turn it from convex to concave. Normally, L_1 is much larger than L_2, therefore, the mismatch of L_1 should be reduced to the lowest level as possible.

Mismatch of R_S:

If R_S in the controller is not accurate, position estimation error may occur. Assuming that the reference current in the d-axis is zero, then the estimation error could be expressed as:

$$\Delta\theta_e(k) \approx \mp\frac{\hat{i}_q \cos\left(4\theta_e(k)\right)}{4\Delta I_H}\frac{1}{\left(\frac{2L_2/T}{\Delta R_S}-1\right)} \tag{28}$$

where ΔR_S is the difference between the real value of rotor resistor and the value used in the digital controller. $\hat{i}_q$ is the current in the estimated q-axis. It is shown that the term $2L_2/T$ has to be much larger than ΔR_S to reduce $\Delta\theta_e(k)$. This condition is relatively not difficult to be satisfied in most machines. (28) also indicates that larger current in the estimated q-axis increases the position estimation error, while larger ΔI_H helps reduce the position estimation error. It has to be noted that $\Delta\theta_e(k)$ alternates from positive to negative all the time, therefore it will be greatly decreased after feeding the estimated position to the PLL observer.

2) HIGH SPEED

During high speed operation, the voltage drop on the inductance and resistor is neglected. Because they is usually small compared to the back-EMF. Therefore, at high speed, the difference between ω_e and $\hat{\omega}_e$ is studied. If ω_e and $\hat{\omega}_e$ don't match in (13), then (13) will become:

$$\begin{aligned} &G\left(\hat{\theta}_e(k),\hat{\omega}_e(k)\right) \\ &\quad\approx {\psi_f}^2\cdot\left(\begin{array}{l}\left(\omega_e(k)-\hat{\omega}_e(k)\right)^2 \\ +4\hat{\omega}_e(k)\,\omega_e(k)\left(\sin\dfrac{\theta_e(k)-\hat{\theta}_e(k)}{2}\right)^2\end{array}\right) \end{aligned} \tag{29}$$

It is shown from (29) that even though $G\left(\hat{\theta}_e(k),\hat{\omega}_e(k)\right)$ will not reach zero, the optimized solution of $\hat{\theta}_e(k)$ is still $\theta_e(k)$. No position estimation error is introduced. The result will be the same if there is mismatch in ψ_f. It has to be noted that if the inductance is considered at high speed, position estimation error may be introduced. But the introduced error is still small.

It has to be noted that even though the proposed position method has some immunity on parameter mismatch, an additional online parameter estimation method is recommended to work together with the proposed position method to improve the robustness of the whole control system.

G. SOLVING THE OPTIMIZATION PROBLEM

Since the convexity of $G\left(\hat{\theta}_e(k),\omega_e(k)\right)$ near $\theta_e(k)$ is guaranteed, the optimization problem could be numerically solved even though noise and parameter mismatch are introduced. Conventional Newton or Quasi-Newton method can be used to solve the problem. However, in digital applications, these methods have problems such as complex calculation of second derivative or vary small divisor. In this paper, a simple method with Taylor expansion is adopted. The $f_e\left(\hat{\theta}_e(k),\hat{\omega}_e(k)\right)$ in (4) could be expanded near $\hat{\theta}_e(k)_{i-1}$ as:

$$\begin{aligned} f_e\left(\hat{\theta}_e(k)_i,\hat{\omega}_e(k)\right) &= f_e\left(\hat{\theta}_e(k)_{i-1},\hat{\omega}_e(k)\right) \\ &\quad +{f_e}'\left(\hat{\theta}_e(k)_i,\hat{\omega}_e(k)\right)\Delta\hat{\theta}_e(k)_i \\ \Delta\hat{\theta}_e(k)_i &= \hat{\theta}_e(k)_i-\hat{\theta}_e(k)_{i-1} \end{aligned} \tag{30}$$

where $i = 1,2,3,\ldots$ is the iteration time and $\hat{\theta}_e(k)_0$ means the initial value of $\hat{\theta}_e(k)$ for calculation. Thus $G\left(\hat{\theta}_e(k)_i,\hat{\omega}_e(k)\right)$ could be expressed as:

$$\begin{aligned} &G\left(\hat{\theta}_e(k)_i,\hat{\omega}_e(k)\right) \\ &\quad= f_e\left(\hat{\theta}_e(k)_i,\hat{\omega}_e(k)\right)^T f_e\left(\hat{\theta}_e(k)_i,\hat{\omega}_e(k)\right) \\ &\quad= {f_e}'\left(\hat{\theta}_e(k)_i,\hat{\omega}_e(k)\right)^T {f_e}'\left(\hat{\theta}_e(k)_i,\hat{\omega}_e(k)\right)\Delta\hat{\theta}_e(k)_i{}^2 \\ &\qquad +2f_e\left(\hat{\theta}_e(k)_{i-1},\hat{\omega}_e(k)\right)^T {f_e}'\left(\hat{\theta}_e(k)_i,\hat{\omega}_e(k)\right)\Delta\hat{\theta}_e(k)_i \\ &\qquad +f_e\left(\hat{\theta}_e(k)_{i-1},\hat{\omega}_e(k)\right)^T f_e\left(\hat{\theta}_e(k)_{i-1},\hat{\omega}_e(k)\right) \end{aligned} \tag{31}$$

${f_e}'\left(\hat{\theta}_e(k)_i,\hat{\omega}_e(k)\right)$ is the derivative of $f_e\left(\hat{\theta}_e(k),\hat{\omega}_e(k)\right)$ at $\hat{\theta}_e(k)_i$ and is expressed as:

$$\begin{aligned} &{f_e}'\left(\hat{\theta}_e(k),\hat{\omega}_e(k)\right) \\ &= \frac{f_e\left(\hat{\theta}_e(k),\hat{\omega}_e(k)\right)}{d\hat{\theta}_e(k)} \\ &= 4\hat{\omega}_e(k)L_2\begin{bmatrix}\cos\left(2\hat{\theta}_e(k)\right) & \sin\left(2\hat{\theta}_e(k)\right) \\ \sin\left(2\hat{\theta}_e(k)\right) & -\cos\left(2\hat{\theta}_e(k)\right)\end{bmatrix} i_{\alpha\beta}(k) \\ &\quad -2L_2\begin{bmatrix}-\sin\left(2\hat{\theta}_e(k)\right) & \cos\left(2\hat{\theta}_e(k)\right) \\ \cos\left(2\hat{\theta}_e(k)\right) & \sin\left(2\hat{\theta}_e(k)\right)\end{bmatrix}\frac{\Delta i_{\alpha\beta}(k)}{T} \\ &\quad +\psi_f\hat{\omega}_e\begin{bmatrix}\cos\left(\hat{\theta}_e(k)\right) \\ \sin\left(\hat{\theta}_e(k)\right)\end{bmatrix} \end{aligned} \tag{32}$$

According to (31), the optimal solution to minimize $G\left(\hat{\theta}_e(k)_i, \hat{\omega}_e(k)\right)$ is

$$\begin{aligned}\Delta\hat{\theta}_e(k)_i &= -\frac{f_e\left(\hat{\theta}_e(k)_{i-1}, \hat{\omega}_e(k)\right)^T f_e'\left(\hat{\theta}_e(k)_i, \hat{\omega}_e(k)\right)}{f_e'\left(\hat{\theta}_e(k)_i, \hat{\omega}_e(k)\right)^T f_e'\left(\hat{\theta}_e(k)_i, \hat{\omega}_e(k)\right)} \\ &= -\frac{f_e\left(\hat{\theta}_e(k)_{i-1}, \hat{\omega}_e(k)\right)^T f_e'\left(\hat{\theta}_e(k)_i, \hat{\omega}_e(k)\right)}{A\left(\hat{\theta}_e(k)_i\right)} \end{aligned} \quad (33)$$

According to the discuss above, $A\left(\hat{\theta}_e(k)_i\right)$ is guaranteed to be larger than zero by either high frequency signal injection or the back-EMF. Therefore $\Delta\hat{\theta}_e(k)_i$ could always be obtained without numerical calculation error. Even if $G\left(\hat{\theta}_e(k)_i, \hat{\omega}_e(k)\right)$ becomes concave because of parameter mismatch, the solution of $\Delta\hat{\theta}_e(k)_i$ is still correct. It has to be noted that $\Delta\hat{\theta}_e(k)_i$ should be limited to a small range to reduce the effects of noise and parameter mismatch. In this paper, $\Delta\hat{\theta}_e(k)_i$ is bounded within $\pm\pi/8$.

After several iterations, the final estimated rotor position at time $t = kT$ is obtained. After obtaining $\hat{\theta}_e(k)$, it is fed into the PLL observer, and the estimated angular speed $\hat{\omega}_e(k)$ as well the the estimated rotor position $\hat{\theta}_{PLL}(k)$ are then obtained.

IV. EXPERIMENTAL VERIFICATION

The effectiveness of the proposed position estimation method is tested on the experimental setup as shown in FIGURE 5. The tested motor is connected with a Dyno. A motor controller is used to drive the tested motor and estimate the rotor position. A resolver is installed on the motor shaft to measure the rotor position. The measured position provided by the resolver is used for comparison. The digital controller is TMS320C28346 provided by TI, and runs at 300 MHz. Thus, it is sufficient to solve the optimization problem in one sampling period. The variables of the algorithm are able to be recorded on an external RAM and then be transferred to the PC for analysis. The parameters of the tested motor and the control algorithm are listed in TABLE 1. The bandwidth of the PLL is set to 10 Hz. Only two iterations are performed to calculate $\hat{\theta}_e(k)$ so that the algorithm does not take too much calculation resources. The proposed position estimation method is firstly tested at standstill, and then on several speeds. At last, the position estimation error on variable speed is provided to verify the effectiveness of the proposed method. It has to be noted that, in this paper, the recorded rotor position is in electrical angle while the recorded rotor speed is in mechanical speed.

A. POSITION ESTIMATION AT ZERO SPEED

Firstly, the effectiveness of the position estimation method at zero speed is tested. Both the reference currents of d-axis and q-axis are set to zero. A 5 kHz square wave with amplitude of 25V is injected into the estimated d-axis so that ΔI_H of about 5 A is generated. Since the sampling noise level of the motor controller is about 0.2 A, the selection of ΔI_H satisfies (24). The conventional polarity determination is performed to determine the initial value of the $\hat{\theta}_e(k)_0$ before start-up. The estimated position $\hat{\theta}_{PLL}(k)$ obtained by the proposed method and the measured position measured from the resolver is shown in FIGURE 6 during start up. It is shown that, the estimated position converges to the measured position in less than 100 ms. Little position estimation error is observed.

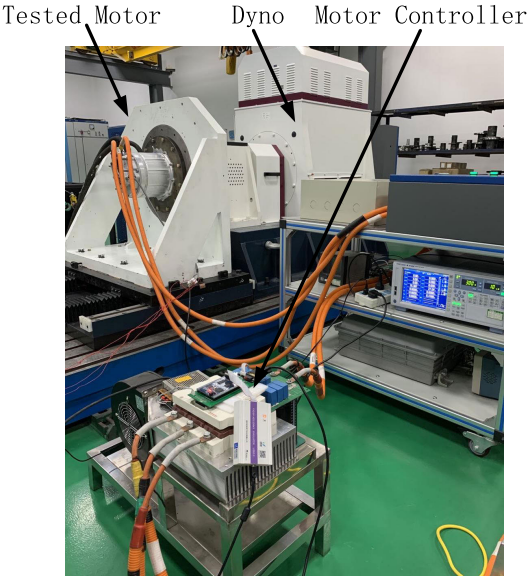

FIGURE 5. Experimental setup.

TABLE 1. Units for magnetic properties.

Symbol	Parameter Name	Parameter Value
R_s	Stator resistor	0.044 Ω
L_d	Inductance in the d-axis	500 μH
L_q	Inductance in the q-axis	1100 μH
ψ_f	Permanent magnet flux linkage	0.058 Wb
p	Pole pairs	4
f_s	Sampling frequency	10 kHz
T	Sampling period	0.0001 s
U_{DC}	DC bus voltage	200 V
K_P	Proportional gain of the PLL	62.8
K_I	Integral gain of the PLL	987

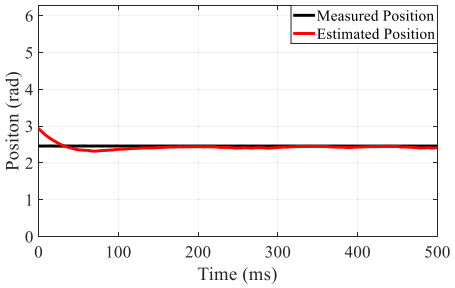

FIGURE 6. The estimated position and measured position at position 2.46 rad.

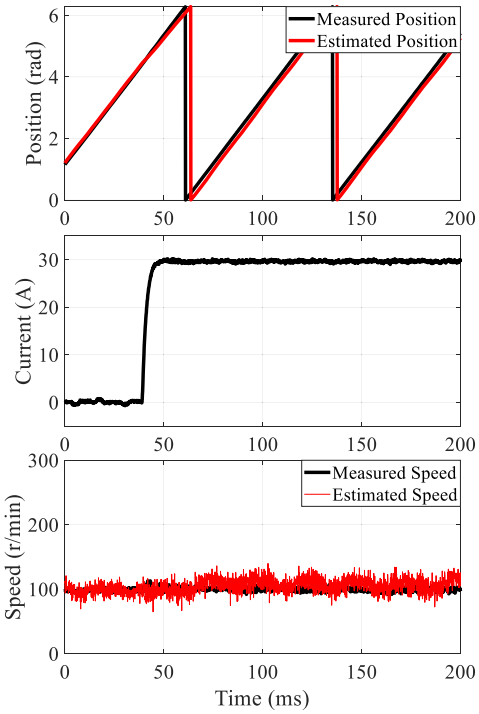

FIGURE 7. The estimated position and measured position, q-axis current, estimated and measured speed at 100 r/min.

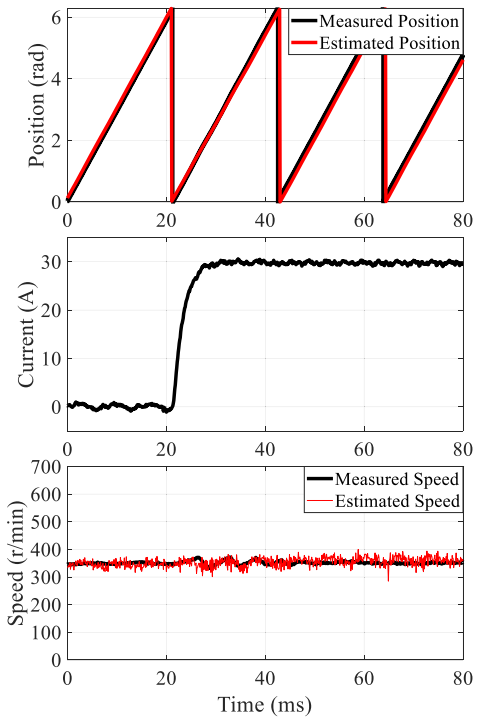

FIGURE 8. The estimated position and measured position, q-axis current, estimated and measured speed at 350 r/min.

B. POSITION AND SPEED ESTIMATION AT MEDIUM AND HIGH SPEED

Then, the proposed position estimation method is tested under different speeds. The tested motor is driven by the Dyno to

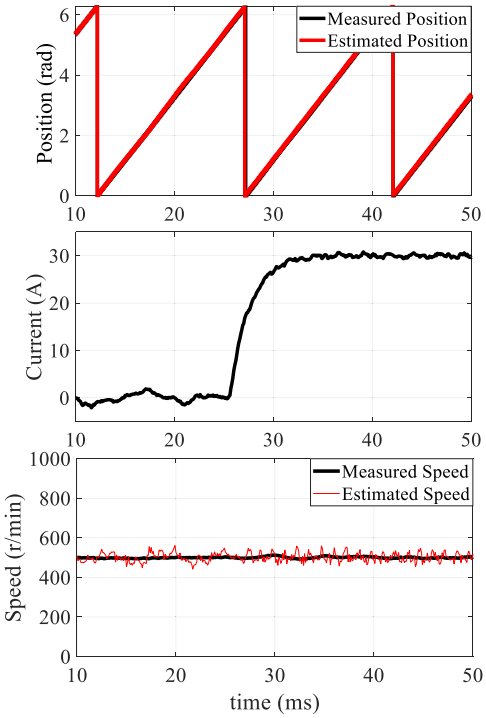

FIGURE 9. The estimated position and measured position, q-axis current, estimated and measured speed at 500 r/min.

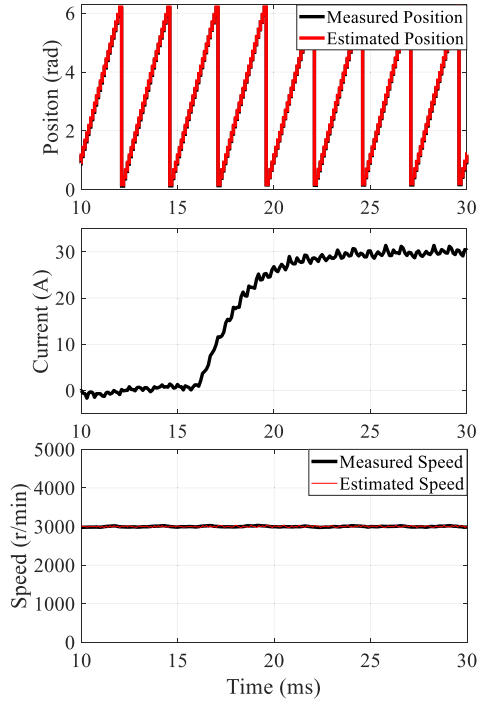

FIGURE 10. The estimated position and measured position, q-axis current, estimated and measured speed at 3000 r/min.

run at different speeds. 30 A current in the estimated q-axis is applied during the test, the estimated and measured position are recorded before and after the application of the q-axis current. According to the parameters of the tested motor, the amplitude of the injected voltage starts to decrease linearly when the motor speed exceeds 325 r/min, and decreases

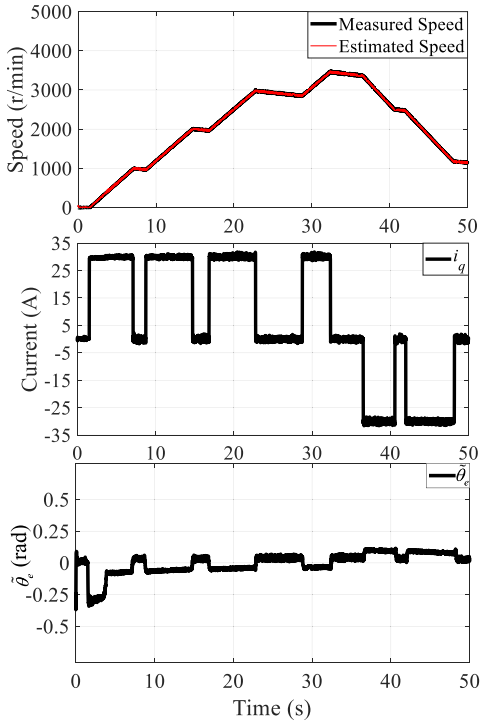

FIGURE 11. The measured speed and estimated speed, q-axis current and position estimation error during acceleration and deceleration.

to zero when the motor speed exceeds 425 r/min. No method switching is needed because of the proposed position estimation method.

The waveform of the estimated position $\hat{\theta}_{PLL}(k)$ and measured position, q-axis current, the estimated and measured speed at different speeds are shown in FIGURE 7, FIGURE 8,FIGURE 9 and FIGURE 10. It is shown that the estimated position follows the measured position very well even if the q-axis current is applied. Also, the estimated speed follows the measured speed very well. At higher speed such as 500 r/min to 3000 r/min, where the back-EMF takes the most significant part, the position estimation error is almost neglectable, no matter there is q-axis current or not, as shown in FIGURE 9 and FIGURE 10. However, as shown in FIGURE 7 and FIGURE 8, it is observed that, at lower speed when high frequency voltage is injected, slight position estimation error appears when q-axis current is applied. This may due to the unmodeled cross coupling between the d-axis and q-axis of the tested motor. Nevertheless, the position estimation error is still acceptable for current control and fault diagnose.

C. POSITION AND SPEED ESTIMATION DURING DYNAMIC PROCESSES

At last, the tested motor is accelerated and decelerated by applying positive and negative q-axis current several times. The process is recorded as shown in FIGURE 11. It is shown that the estimated speed matches the measured speed very well during acceleration and deceleration.

The position estimation error is maintained in very small range. The position estimation error is a little bit larger when high frequency voltage injection is adopted at low speed. The slight estimation error may due to the mismatch of the motor parameters between the model used in the controller and the real motor. No speed oscillation could be observed when high frequency voltage injection is removed. Thus, the effectiveness of the proposed full-speed-range position and speed estimation method is verified.

V. CONCLUSION

This paper proposes a full-speed-range position estimation method for IPMSM. The position estimation problem is converted to solving a single variable simplified quadratic optimization problem. The convexity of the cost function is checked at different cases to make sure that the optimization problem is solvable. The sensitivity of sampling noise and parameter mismatch are discussed to check the robustness of the proposed method. The high frequency injection signal at standstill and low speed is also discussed in detail, and it is concluded that high frequency square wave voltage signal best suite for the proposed method. Experiments are carried out to verify the effectiveness of the proposed position estimation method. The method is tested under both steady state and dynamic state, the results show that the proposed method have good tracking performance on both rotor position and speed.

ACKNOWLEDGMENT

This article was presented in part at the 2019 22nd International Conference on Electrical Machines and Systems (ICEMS), Harbin, China, in August 2019, (Position Sensorless Control of IPMSM Based on Quasi-Newton Methods).

REFERENCES

[1] N. K. Quang, N. T. Hieu, and Q. P. Ha, "FPGA-based sensorless PMSM speed control using reduced-order extended Kalman filters," *IEEE Trans. Ind. Electron.*, vol. 61, no. 12, pp. 6574–6582, Dec. 2014, doi: 10.1109/TIE.2014.2320215.

[2] C. Moon, J. S. Han, and Y. A. Kwon, "Square-root unscented Kalman filter for state estimation of permanent magnet synchronous motor," in *Proc. 55th Annu. Conf. Soc. Instrum. Control Engineers Jpn. (SICE)*, Sep. 2016, pp. 460–464, doi: 10.1109/SICE.2016.7749203.

[3] A. Piippo, M. Hinkkanen, and J. Luomi, "Adaptation of motor parameters in sensorless PMSM drives," *IEEE Trans. Ind. Appl.*, vol. 45, no. 1, pp. 203–212, 2009, doi: 10.1109/TIA.2008.2009614.

[4] K. H. Nam, J. S. Park, C. Moon, and Y. A. Kwon, "Sensorless speed control of permanent magnet synchronous motor based on novel adaptive control with compensated parameters," in *Proc. IEEE Region 10 Conf. (TENCON)*, Oct. 2014, pp. 1–4, doi: 10.1109/TENCON.2014.7022475.

[5] E.-K. Kim, J. Kim, H. T. Nguyen, H. H. Choi, and J.-W. Jung, "Compensation of parameter uncertainty using an adaptive sliding mode control strategy for an interior permanent magnet synchronous motor drive," *IEEE Access*, vol. 7, pp. 11913–11923, 2019, doi: 10.1109/ACCESS.2019.2892749.

[6] K.-G. Lee, J.-S. Lee, and K.-B. Lee, "SPMSM sensorless control for wide speed range using full-order flux observer," in *Proc. IEEE Int. Conf. Ind. Technol. (ICIT)*, Feb. 2014, pp. 164–168, doi: 10.1109/ICIT.2014.6894932.

[7] L. Sheng, W. Li, Y. Wang, M. Fan, and X. Yang, "Sensorless control of a shearer short-range cutting interior permanent magnet synchronous motor based on a new sliding mode observer," *IEEE Access*, vol. 5, pp. 18439–18450, 2017, doi: 10.1109/ACCESS.2017.2734699.

[8] W. Liu, S. Chen, and H. Huang, "Adaptive nonsingular fast terminal sliding mode control for permanent magnet synchronous motor based on disturbance observer," *IEEE Access*, vol. 7, pp. 153791–153798, 2019, doi: 10.1109/ACCESS.2019.2948945.
[9] X. Liu, H. Yu, J. Yu, and L. Zhao, "Combined speed and current terminal sliding mode control with nonlinear disturbance observer for PMSM drive," *IEEE Access*, vol. 6, pp. 29594–29601, 2018, doi: 10.1109/ACCESS.2018.2840521.
[10] Y. Liu, J. Yu, H. Yu, C. Lin, and L. Zhao, "Barrier Lyapunov functions-based adaptive neural control for permanent magnet synchronous motors with full-state constraints," *IEEE Access*, vol. 5, pp. 10382–10389, 2017, doi: 10.1109/ACCESS.2017.2713419.
[11] H. Chaoui, W. Gueaieb, and M. C. E. Yagoub, "Neural network based speed observer for interior permanent magnet synchronous motor drives," in *Proc. IEEE Electr. Power Energy Conf. (EPEC)*, Oct. 2009, pp. 1–6, doi: 10.1109/EPEC.2009.5420924.
[12] N. Li, L. Dong, Y. You, Y. Gao, and X. Liao, "Initial rotor position estimation of IPMSM based on improved rotating high frequency signal injection," in *Proc. IEEE Conf. Expo Transp. Electrific. Asia–Pacific (ITEC Asia–Pacific)*, Aug. 2014, pp. 1–4, doi: 10.1109/ITEC-AP.2014.6940935.
[13] T.-H. Liu, S.-K. Tseng, T.-W. Lin, and J.-L. Chen, "Sensorless IPMSM position control system using a high frequency injection method," in *Proc. IEEE 2nd Annu. Southern Power Electron. Conf. (SPEC)*, Dec. 2016, pp. 1–6. [Online]. Available: http://ieeexplore.ieee.org/document/7845526/, doi: 10.1109/SPEC.2016.7845526.
[14] J. Zhao, S. Nalakath, and A. Emadi, "A high frequency injection technique with modified current reconstruction for low-speed sensorless control of IPMSMs with a single DC-link current sensor," *IEEE Access*, vol. 7, pp. 136137–136147, 2019. [Online]. Available: https://ieeexplore.ieee.org/document/8843981/, doi: 10.1109/ACCESS.2019.2942148.
[15] S. Wang, K. Yang, and K. Chen, "An improved position-sensorless control method at low speed for PMSM based on high-frequency signal injection into a rotating reference frame," *IEEE Access*, vol. 7, pp. 86510–86521, 2019. [Online]. Available: https://ieeexplore.ieee.org/document/8746146/, doi: 10.1109/ACCESS.2019.2925214.
[16] H. Gao, Y. Yu, J. Bao, C. Li, and S. Cheng, "Initial rotor position estimation of an IPMSM based on PWM inverter carrier frequency component," in *Proc. Int. Conf. Electr. Mach. Syst.*, Aug. 2011, pp. 1–4, doi: 10.1109/ICEMS.2011.6073958.
[17] M. Mamo, K. Ide, M. Sawamura, and J. Oyama, "Novel rotor position extraction based on carrier frequency component method (CFCM) using two reference frames for IPM drives," *IEEE Trans. Ind. Electron.*, vol. 52, no. 2, pp. 508–514, Apr. 2005. [Online]. Available: http://ieeexplore.ieee.org/document/1413558/, doi: 10.1109/TIE.2005.844234.
[18] D. Xu, B. Wang, G. Zhang, G. Wang, and Y. Yu, "A review of sensorless control methods for AC motor drives," *CES Trans. Elect. Mach. Syst.*, vol. 2, no. 1, pp. 104–115, Mar. 2018, doi: 10.23919/TEMS.2018.8326456.
[19] G. Bisheimer, M. O. Sonnaillon, C. H. De Angelo, J. A. Solsona, and G. O. Garcia, "Full speed range permanent magnet synchronous motor control without mechanical sensors," *IET Electr. Power Appl.*, vol. 4, no. 1, pp. 35–44, Jan. 2010, doi: 10.1049/iet-epa.2008.0187.
[20] W. T. Villet, M. J. Kamper, P. Landsmann, and R. Kennel, "Hybrid position sensorless vector control of a reluctance synchronous machine through the entire speed range," in *Proc. 15th Int. Power Electron. Motion Control Conf. (EPE/PEMC)*, Sep. 2012, pp. LS4b-1.1–1–LS4b-1.1-7, doi: 10.1109/EPEPEMC.2012.6397450.
[21] G. Wang, R. Yang, and D. Xu, "DSP-based control of sensorless IPMSM drives for wide-speed-range operation," *IEEE Trans. Ind. Electron.*, vol. 60, no. 2, pp. 720–727, Feb. 2013, doi: 10.1109/TIE.2012.2205360.
[22] M. Z. Liu Jilong, X. Fei, and G. Shan, "Hybrid position-sensorless control scheme for PMSM based on combination of IF control and sliding mode observer," *Trans. China Electrotech. Soc.*, vol. 33, no. 4, pp. 919–929, 2018. [Online]. Available: http://dgjsxb.ces-transaction.com/EN/abstract/article_5038.shtml, doi: 10.19595/j.cnki.1000-6753.tces.161597.
[23] Y. Sun, M. Preindl, S. Sirouspour, and A. Emadi, "Unified wide-speed sensorless scheme using nonlinear optimization for IPMSM drives," *IEEE Trans. Power Electron.*, vol. 32, no. 8, pp. 6308–6322, Aug. 2017, doi: 10.1109/TPEL.2016.2621064.
[24] S. Nalakath, Y. Sun, M. Preindl, and A. Emadi, "Optimization-based position sensorless finite control set model predictive control for IPMSMs," *IEEE Trans. Power Electron.*, vol. 33, no. 10, pp. 8672–8682, Oct. 2018, doi: 10.1109/TPEL.2017.2784816.
[25] Z. Wang, B. Xie, L. Bu, W. Liu, F. Peng, and Y. Huang, "Position sensorless control of IPMSM based on quasi-Newton methods," in *Proc. 22nd Int. Conf. Electr. Mach. Syst. (ICEMS)*, Aug. 2019, pp. 1–6, doi: 10.1109/ICEMS.2019.8921877.

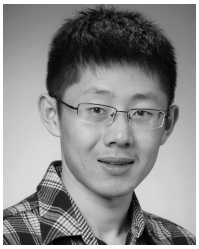

FEI PENG (Member, IEEE) received the B.S. and M.S. degrees in electrical engineering from Southeast University, Nanjing, China, in 2010 and 2012, respectively, and the Ph.D. degree from McMaster University, Hamilton, ON, Canada in 2016. He worked as a Postdoctoral Fellow with the McMaster Institute for Automotive Research and Technology (MacAUTO), McMaster University. Since December 2016, he has been an Assistant Professor with the School of Electrical Engineering, Southeast University. His research interests include optimal design and control of power converters and modeling and digital control of motor drives.

YU YAO (Graduate Student Member, IEEE) received the B.S. degree in electrical engineering from Southeast University, Nanjing, China, in 2016, where he is currently pursuing the Doctor of Engineering degree in electric machines and control with the School of Electrical Engineering. His main research interests include design of the power inverter, current regulator design, position sensorless drive for the high-speed PSMSM, and drive system with LCL output filter.

ZHIYU WANG received the B.S. degree in electrical engineering from Southeast University, Nanjing, China, in 2017, where he is currently pursuing the master's degree. His main research interest includes control of PM machine drives.

YUNKAI HUANG (Member, IEEE) received the M.Sc. and Ph.D. degrees in electrical engineering from Southeast University, Nanjing, China, in 2001 and 2007, respectively. He is currently a Professor with the School of Electrical Engineering, Southeast University. His research interests include design and control of PM machine and high-speed machine, applications in domestic appliances, electric vehicles, railway traction, all-electric ships, more-electric aircraft, and wind power generation systems.

HUI YANG (Member, IEEE) was born in Changning, Hunan, China. He received the B.Eng. degree in electrical engineering from the Dalian University of Technology, Dalian, China, in 2011, and the Ph.D. degree in electrical engineering from Southeast University, Nanjing, China, in 2016.

From 2014 to 2015, he was supported by the China Scholarship Council through a one-year joint Ph.D. studentship with The University of Sheffield, Sheffield, U.K. Since 2016, he has been with Southeast University, where he has been an Associate Professor with the School of Electrical Engineering. Since 2019, he has been a Postdoctoral Fellow with the School of Electrical Engineering, The Hong Kong Polytechnic University. He is the holder of 14 patents. His research interests include design and analysis of novel permanent-magnet machines with particular reference to variable-flux machines for electric vehicles and renewable energy applications. He was a recipient of the Best Paper Awards in ICEMS 2014, EVER 2015, and ICEMS 2019.

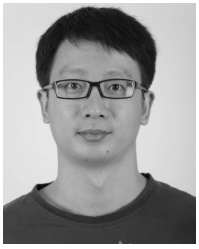

BINGRUO XIE received the B.S. and Ph.D. degrees in electrical engineering from the Huazhong University of Science and Technology, Wuhan, China, in 2004 and 2010, respectively. Since July 2010, he has been an Assistant Research Fellow with the Locomotive and Car Research Institute, China Academy of Railway Sciences, Beijing, China. He held the position of Associate Research Fellow, in April 2016. His research interest includes design and control of traction drive systems.